Bone 120 (2019) 465–475

Contents lists available at ScienceDirect

Bone

journal homepage: www.elsevier.com/locate/bone

Full Length Article

Osteocytes reflect a pro-inflammatory state following spinal cord injury in a rodent model

Corinne E. Metzger[a,*], Sammy Gong[b], Miriam Aceves[b], Susan A. Bloomfield[a], Michelle A. Hook[b]

[a] Department of Health and Kinesiology, Texas A&M University, College Station, TX, United States of America
[b] Department of Neuroscience and Experimental Therapeutics, Texas A&M Health Science Center, Bryan, TX, United States of America

ARTICLE INFO

Keywords:
Spinal cord injury
Inflammation
Osteocytes
Cytokines

ABSTRACT

Profound bone loss occurs following spinal cord injury (SCI) resulting in a high incidence of fractures. While likely caused in part by loss of weight-bearing, there is greater bone loss following SCI when compared to that observed in other disuse animal models. Patients with SCI have a protracted inflammatory response, with elevated circulating levels of pro-inflammatory markers. This chronic inflammation could compound the bone loss attributed to disuse and the loss of neural signaling. To assess this, we examined inflammatory markers and bone turnover regulators in osteocytes from rats with a moderate spinal contusion injury (SCI) and intact controls (CON). We counted osteocytes positive for cytokines [tumor necrosis factor-α (TNF-α), interleukin-6 (IL-6), and interleukin-17 (IL-17), and interleukin-10 (IL-10)], osteoclastogenesis regulators RANKL and OPG, and the bone formation inhibitor sclerostin, 32 days after the spinal contusion. By day 9 post-injury, the majority of SCI rats had recovered significant locomotor function and were bearing weight on their hindlimbs. However, despite weight-bearing, peripheral QCT scans demonstrated lower bone mass due to SCI in the proximal tibia metaphysis compared to CON. SCI animals also had lower cancellous bone volume, lower bone formation rate (BFR), lower osteoid surface (OS), and higher osteoclast surface (Oc.S). Tibial mid-shaft periosteal BFR was also lower after SCI. Immunohistochemical staining of the distal femur bone revealed cancellous osteocytes positive for TNF-α, IL-6, IL-17, and IL-10 were elevated in SCI animals relative to intact controls. Protein expression of RANKL+, OPG+, and sclerostin+ osteocytes was also higher in SCI rats. At the cortical midshaft, osteocyte TNF-α, IL-6, and sclerostin were statistically higher in SCI vs. CON. With regression analysis, inflammatory factors were associated with changes in bone turnover. In conclusion, inflammatory factors as well as altered mechanical loading influence bone turnover following a moderate SCI. Treatments aimed at minimizing fracture risk after SCI may need to target both the chronically altered inflammatory state as well as disuse-induced bone loss.

1. Introduction

Spinal cord injury (SCI) leads to profound musculoskeletal losses with deficits in bone mass evolving rapidly in the first months after injury [1]. SCI patients have 40–70% lower bone mass relative to age-matched comparator values in cancellous–rich bone sites [2,3], and 25–35% lower bone mass in cortical sites like the shafts of the tibia [3]. Within the first 6–12 months following complete SCI, the rate of bone loss is approximately 1% per week, a much greater rate of bone loss than that observed during bed rest at approximately 0.1% per week [4]. Evidence from a study examining monozygotic twin pairs, one with motor complete SCI and one without, demonstrated that length of time from SCI, not age, was linearly related to the degree of bone loss indicating the potential for persistent loss of bone mass extending beyond the acute injury [5]. Overall, this significant loss of bone leads to a high frequency of low energy fractures [6], with an estimated 50% of SCI patients sustaining a low trauma or osteoporotic fracture post-injury [7]. Fracture incidence increases with time after injury [8].

Rodent models of SCI demonstrate similarly rapid bone loss with large decreases in cancellous bone volume and deterioration of cancellous microarchitecture [9–14]. The mechanical strength of the bone is decreased in these SCI rodents compared to controls by up to 50% three weeks after injury [15], consistent with the increased risk for fracture seen in human patients. These animal models also demonstrate decreased bone formation rate due to SCI [12,14], increased osteoclast differentiation markers, and decreased osteoblast differentiation markers [13]. Additionally, scanning electron microscopy of bone tissue of rats 8 weeks after complete SCI demonstrated reduced osteocyte

* Corresponding author.
E-mail addresses: metzgercorinne@gmail.com (C.E. Metzger), hook@medicine.tamhsc.edu (M.A. Hook).

https://doi.org/10.1016/j.bone.2018.12.007
Received 17 August 2018; Received in revised form 6 December 2018; Accepted 10 December 2018
Available online 11 December 2018

density, a lower number of osteocyte dendritic processes, and altered osteocyte morphology [12]. Given that osteocytes are key regulators and signaling cells in bone tissue [16], these changes in osteocyte morphology likely contribute to subsequent changes in bone mass. Interestingly, compared to the extent of bone loss in hindlimb cast immobilization or neurectomy models, there is greater bone loss and more profound decrements in mechanical properties following SCI [17,18]. These observations suggest that a lack of mechanical loading and the loss of neural signaling are not the only contributors to impaired bone integrity following SCI.

One factor that could accelerate bone loss following SCI is the protracted pro-inflammatory response and immune dysfunction seen in patients [19]. Bone loss is a common comorbidity in many conditions that involve chronic systemic inflammation, including inflammatory bowel disease [20], psoriasis [21], rheumatoid arthritis [22], and systemic lupus erythematosus [23]. After SCI, approximately 47% of patients are diagnosed with acute systemic inflammatory response syndrome (SIRS) at hospital admission [24], a condition that contributes to a high incidence of secondary organ complications [25]. Importantly, this inflammation persists well beyond the acute phase in the emergency room. C-reactive protein (CRP), a generalized indicator of inflammation, is elevated in SCI patients [26,27], with the highest CRP values observed in those with quadriplegia versus paraplegia measured approximately 14 years post-injury [28]. Similarly, SCI patients exhibit elevated serum Th1 cytokines, tumor necrosis factor-α (TNF-α) and interleukin-6 (IL-6), compared to able-bodied controls, for years following injury [29,30]. In a rodent SCI model, we have also shown increased circulating pro-inflammatory cytokines 25 days after a moderate SCI, relative to intact controls [31]. These pro-inflammatory factors, like TNF-α and IL-6, stimulate an increase in osteoclastogenesis and suppress bone formation, as well as activate other regulators of bone cell activity like receptor activator of nuclear factor KB ligand (RANKL) and sclerostin [32–34]. The inflammatory response inherent to SCI could enhance bone loss and/or limit the ability to recover bone mass post-injury.

The goal of this current study is to examine the inflammatory status of bone following a moderate T12 spinal contusion injury in young male rats. Previously, we examined the role of osteocytes in the context of systemic inflammation caused by chronic inflammatory bowel disease [35]. In that rodent model, we found elevated osteocyte TNF-α and IL-6 corresponding with high osteocyte sclerostin, RANKL, and OPG. These factors were strongly correlated with high osteoclast surfaces and low bone formation rate [35]. Additionally, we have previously shown that osteocyte IL-6 and sclerostin, but not osteocyte TNF-α, are altered by mechanical loading and unloading [36]. Therefore, we aimed to understand the role of both inflammation and altered mechanical loading on osteocyte proteins following SCI. We hypothesized that elevations in osteocyte pro-inflammatory cytokines (TNF-α and IL-6), RANKL, OPG, and sclerostin in SCI would be associated with high osteoclast surface and depressed bone formation rate. Further, we hypothesized that both locomotor ability and inflammatory cytokines would predict the degree of changes in bone turnover.

2. Materials and methods

2.1. Animals

Male Sprague-Dawley rats obtained from Envigo (Houston, TX), approximately 90–110 days old (300–350 g), were individually housed in Plexiglas bins [45.7 (length) × 23.5 (width) × 20.3 (height) cm] with food (Teklad 2018; Envigo, Houston, TX) and water continuously available. Animals were divided into intact controls (CON) and spinal contusion (SCI) groups (n per group = 6). SCI animals were monitored for weight on days that they were assessed for locomotor function, and were checked daily for signs of autophagia and spastic hypertonia. An animal was classified as having spastic hypertonia if a limb was in an extended, fixed position and was resistant to movement. Bladders were manually expressed in the morning (8–9.30 a.m.) and evening (6–7.30 p.m.) until subjects regained bladder control, which was operationally defined as three consecutive days with an empty bladder at the time of expression. The rats were maintained on a 12 h light/dark cycle and tested during the last 6 h of the light cycle. Fluorochrome calcein labels were injected 7 and 2 days prior to euthanasia for assessment of mineralizing surfaces. Thirty-two days post-injury, all animals were humanely euthanized with a lethal injection of pentobarbital (100 mg/kg), perfused with paraformaldehyde, and bone tissue was collected. All of the experiments were reviewed and approved by the institutional animal care committee at Texas A&M University and all NIH guidelines for the care and use of animal subjects were followed.

2.2. Surgery

SCI animals had a moderate contusion injury at vertebral level T12. For the spinal contusion injury, the rats were anesthetized with inhaled isoflurane (5% to induce anesthesia and 2–3% for maintenance). The rat's back was shaved and disinfected with iodine and a 5.0 cm incision was made over the spinal cord. Two incisions were made along the vertebral column, on each side of the dorsal spinous processes, extending about 2 cm rostral and caudal to the T12 segment. Muscle and connective tissue were then dissected to expose the underlying vertebral segments. Musculature around the transverse processes was cleared to allow for clamping of the vertebral spinal column. Next, the dorsal spinous process at T12 was removed, and the spinal tissue exposed. The dura remained intact. The vertebral column was fixed within the Infinite Horizons impactor (Precision Systems Instrumentation) using two pairs of Adson forceps. A moderate injury was produced using an impact force of 150 kdyn and a 1 s dwell time. The wound was closed with Michel clips. For the first 24-h after surgery, the rats were housed in a recovery room. All subjects were treated with 100,000 U/kg penicillin G potassium (intraperitoneal injection) immediately after surgery and again 2 days later. No post-operative pain medications or NSAIDS were given as inflammation was the primary outcome of the study. To facilitate access to the food and water after spinal surgery, extra bedding was added to the housing bins and long mouse sipper tubes were used so that the rats could reach the water without rearing. To help maintain hydration, the subjects were also given 3.0 ml of saline (0.9%, i.p.) following surgery.

2.3. Assessment of locomotor recovery

Locomotor behavior was assessed using the Basso-Beattie-Bresnahan (BBB) rating scale [37] in an open enclosure (99 cm diameter and 23 cm deep). The subjects were acclimated to the apparatus for 5 min per day for 3 days prior to surgery. Using this scale, no movement of the hindlimbs (ankle, knee or hip) is designated a score of 0, and intermediate milestones include slight movement of one joint [1], extensive movement of all three joints [7], occasional weight supported stepping in the absence of coordination [10], and consistent weight supported stepping with consistent FL-HL coordination [14]. Higher scores reflect consistent limb co-ordination and improved fine motor skill. Twenty-four hours after surgery, each subject was placed in the open field and observed for 4 min to assess locomotor function. Scoring occurred on days 1, 2, 3, 4, 5, 6, 7, 9, 11, 13, 15, 18, 21, 24, 27, and 30 post-injury. All observers had high intra- and inter-observer reliability (all r's > 0.89) and were blind to the subjects' experimental treatment.

2.4. Peripheral quantitative computed tomography

Right femurs and tibia were saved in phosphate buffered saline at −35 °C. Once thawed, ex vivo pQCT scans of the proximal tibia metaphysis and distal femur metaphysis (mixed cortical and cancellous bone site) and mid-shaft tibia and midshaft femur (purely cortical bone

site) were completed on a Stratec XCT Research-M device (Norland Corp., Fort Atkinson, WI). Metaphyseal volumetric BMD was measured at the proximal tibia and distal femur from 4 slices located at least 1 mm distal to the growth plate. Three contiguous slices were averaged to provide one value for each variable at the proximal tibia metaphysis. One midshaft tibia and midshaft femur slice was taken at approximately 50% of the total bone length. Scans were completed at 2.5 mm/s scan speed, 100 μm voxel resolution, and 0.5 mm slice thickness. Measures obtained from the ex vivo pQCT scans include cortical and cancellous bone mineral content (BMC), volumetric bone mineral density (vBMD), and midshaft tibia cortical thickness.

2.5. Dynamic and static cancellous histomorphometry

For cancellous histomorphometry, undemineralized left proximal tibia were fixed in 4% phosphate-buffered formalin for 12 h and then subjected to serial dehydration and embedded in methyl methacrylate (J.T.Baker, VWR, Radnor, PA, USA). Serial frontal sections were cut 8 μm-thick and left unstained for fluorochrome calcein label measurements. The histomorphometric analyses were performed using OsteoMeasure Analysis System, version 3.3 (OsteoMetrics, Inc., Atlanta, GA, USA). A defined region of interest was established approximately 500 μm from the growth plate and within the endocortical edges encompassing approximately 8 mm^2 at 20× magnification. Total bone surface (BS), single-labeled surface (sLS/BS), double-labeled surface (dLS/BS), mineralizing surface (MS/BS), and interlabel distances were measured at 20× magnification. Mineral apposition rate (MAR) was calculated from the interlabel distance and time of labels. Bone formation rate (BFR/BS) was determined by multiplying MS/BS by MAR. Additionally, 4 μm-thick sections were treated with von Kossa stain and tetrachrome counterstain to measure cancellous microarchitecture (% BV/TV, Tb. Th, Tb. Sp, and Tb. N) and osteoid (OS/BS) and osteoclast (Oc.S/BS) surfaces, expressed as a percent of total cancellous surface measured at 40× magnification. Two non-contiguous sections were analyzed and averaged for all histomorphometric measures. All analyses were completed by the same individual to reduce variability. Nomenclature for cancellous histomorphometry follows standard usage guidelines [38].

2.6. Dynamic cortical histomorphometry

Undemineralized left distal tibia were fixed in 4% phosphate-buffered formalin for 12 h and then serially dehydrated and embedded in methyl methacrylate. Cross sections of the bone closest to the mid-shaft were made on an IsoMet Low Speed Saw (Buehler, Lake Bluff, IL) approximately 100 μm thick. Cross sections were analyzed at both the periosteal and endocortical surface at 20× magnification using OsteoMeasure Analysis System, version 3.3 (OsteoMetrics, Inc., Atlanta, GA, USA) for MS/BS and MAR; bone formation rate was calculated as stipulated above.

2.7. Immunohistochemistry

Left distal femora were fixed in 4% phosphate-buffered formalin for 12 h at 4 °C, decalcified in a sodium citrate/formic acid solution for approximately 18 days and then stored in 70% ethanol. Sections were then further dehydrated in Thermo-Scientific STP 120 Spin Tissue Processor, paraffinized via a Thermo Shandon Histocenter 3 Embedding tool, sectioned to approximately 8 μm thickness, mounted on positively charged slides, and immunostained using an avidin-biotin method as previously described [35]. Sections were incubated overnight at 4 °C with primary antibodies: polyclonal rabbit anti-rat TNF-α, (1:100, LifeSpan BioSciences, Inc., Seattle, WA), polyclonal rabbit anti-IL-6 (1:300, Abcam, Cambridge, MA), polyclonal rabbit anti-IL-10 (1:300, Abcam), polyclonal goat anti-mouse sclerostin (1:100, R&D Systems, Minneapolis, MN), polyclonal rabbit anti-IL-17 (1:150, Abcam), polyclonal rabbit anti-RANKL (1:200, Abcam), and polyclonal rabbit anti-OPG (1:100, Biorbyt, San Francisco, CA). Negative controls for all antibodies were completed by omitting the primary antibody. Sections were analyzed by quantifying the proportion of all osteocytes staining positively for the protein in the cancellous bone of the metaphysis (~500 μm from the growth plate, an area of approximately 4 mm^2) and the cortical bone near the midshaft (an area of approximately 2 mm^2). Negative controls (still containing methyl green stain) were used to quantify osteocyte density. Osteocyte density was quantified two ways – per tissue area (mm^2) and normalized to the bone area of the same sample.

2.8. Statistical analyses

A *t*-test was completed between CON and SCI for each variable. A repeated measures ANOVA was used to compare BBB scores between groups and across time with a Sidak pairwise comparison post hoc. Statistical significance was determined at $p < 0.05$. Effect size (partial eta-squared) was determined for values of $p < 0.05$. Linear regression was completed with osteoclast surface as the dependent variable and independent factors as TNF-α, IL-6, IL-17, RANKL, and OPG and, separately, with bone formation rate as the dependent variable and the independent factor as and sclerostin. Additionally, linear regression for factors predicting sclerostin (BBB scores and TNF-α) was used. A new model for multiple linear regression between these factors was accepted when the adjusted R^2 increased and all slopes in the model were significant ($p < 0.05$). If these criteria were not met, the previous model was accepted. All data is represented as mean ± standard deviation. Statistical analyses were completed on IBM SPSS Statistics Version 23 (IBM; Armonk, NY).

3. Results

3.1. Thirty days after spinal contusion, SCI animals were supporting weight on both hindlimbs, but mobility was still lower compared to CON

SCI animals lost an average of 4% of their baseline body weight within seven days of the contusion injury, but gained weight following that point ending with 7% greater body weight than baseline. For locomotor scores, with repeated measures, there were significant effects of time, time by group, and between subjects ($p < 0.0001$). The SCI subjects recovered locomotor function across time, but at all time points the SCI subjects had lower average BBB scores than CON ($p < 0.0001$; Fig. 1). By day 9 following injury, the majority of SCI animals were

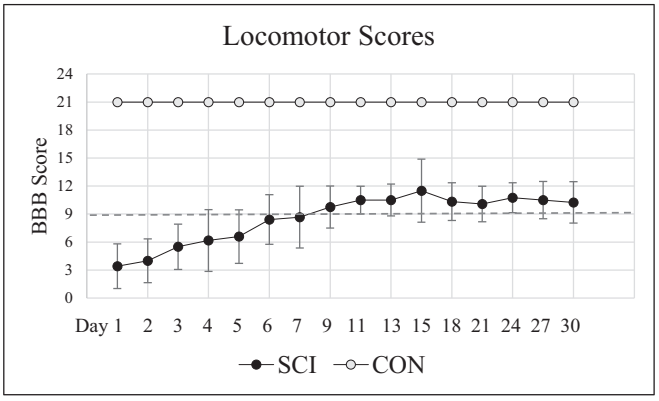

Fig. 1. BBB locomotor scores were lower for SCI rats with recovery of weight bearing ability by day 9 following SCI. Dashed line indicates score of weight bearing (BBB = 9). CON rats were fully mobile (BBB = 21). Error bars on SCI values = standard deviation. SCI animals had statistically lower BBB scores than CON at all time points ($p < 0.0001$). SCI animals were statistically lower than CON at all timepoints.

Table 1
pQCT measures of the proximal tibia metaphysis and distal femur metaphysis assessed 32 days after moderate contusion injury at T12.

	Proximal tibia		Distal femur	
	CON	SCI	CON	SCI
Total BMC (g)	10.45 ± 1.3	8.40 ± 1.1*	10.6 ± 1.0	9.47 ± 0.6#
Total vBMD (mg/cm^3)	547.85 ± 40.9	510.47 ± 43.6	661.75 ± 31.2	636.25 ± 40.4
Cancellous vBMD (mg/cm^3)	294.03 ± 62.6	221.06 ± 33.2*	326.62 ± 53.9	307.27 ± 28.3
Metaphyseal Cortical vBMD (mg/cm^3)	557.88 ± 37.7	524.55 ± 40.5	667.41 ± 28.79	637.89 ± 43.3
Total area (mm^2)	19.09 ± 2.2	16.46 ± 0.8*	16.00 ± 0.7	15.00 ± 1.0

Data are represented as mean ± standard deviation.
* Difference from CON, $p < 0.05$.
# Trending difference from CON, $p = 0.078$.

weight-bearing on the hindlimbs. They had recovered to BBB scores of 9.75 ± 2.2 (mean ± SD). By day 30 post-injury, the mean SCI scores were 10.25 ± 2.2, indicating occasional weight-supported plantar steps with no forelimb/hindlimb coordination.

3.2. SCI caused decrements in bone mass and area at the proximal tibia metaphysis

pQCT scans of the proximal tibia metaphysis demonstrated statistically lower total BMC ($p = 0.017$, effect size = 0.448), cancellous vBMD ($p = 0.03$, effect size = 0.388), and total area ($p = 0.024$, effect size = 0.413) in SCI vs. CON animals (Table 1). Small deficits in bone mineral content at the distal femur metaphysis in SCI rats did not reach statistical significance ($p = 0.078$).

3.3. Declines in cortical bone mass were seen in the midshaft tibia and femur following SCI

Total area of the midshaft femur was significantly lower in SCI rats than in intact controls ($p = 0.006$, effect size = 0.630; Table 2). There were also trends for decreased cortical BMC after SCI in both midshaft tibia and femur, but these did not reach statistical significance ($p = 0.086$, $p = 0.073$, respectively). Similarly, cortical thickness was lower in the tibia following SCI, although not significantly ($p = 0.057$). There were no statistical differences observed in cortical vBMD at either site.

3.4. Deficits in cancellous microarchitecture after SCI correspond with increased osteoclast surface and decreased osteoid surface

%BV/TV measured by static histomorphometry at the proximal tibia metaphysis was 55% lower in SCI vs. CON ($p < 0.001$, effect size = 0.702; Fig. 2A). Trabecular thickness and trabecular number were also lower in SCI animals ($p = 0.004$, effect size = 0.584; $p = 0.001$, effect size = 0.657, respectively; Fig. 2B, D) and trabecular separation was higher compared to CON ($p = 0.002$, effect size = 0.622 l; Fig. 2C). Percent osteoid surface was lower ($p = 0.034$, effect size = 0.377; Fig. 2E), and %osteoclast surface almost 2.5-fold higher ($p < 0.0001$, effect size = 0.795; Fig. 2F) in SCI animals.

3.5. Both cancellous and periosteal cortical bone formation rates were depressed after SCI

Dynamic histomorphometry at the proximal tibia metaphysis revealed 37% lower cancellous BFR/BS in SCI animals ($p = 0.002$, effect size = 0.634; Fig. 3C). This impact on BFR/BS was associated with a 45% lower mineralizing surface (%MS/BS) in SCI vs. CON ($p < 0.0001$, effect size = 0.825; Fig. 3A) with a mineral apposition rate (MAR) that was not statistically different from CON ($p = 0.084$; Fig. 3B). Reductions in periosteal BFR/BS were also observed at the midshaft tibia ($p < 0.0001$, effect size = 0.778; Fig. 4A) due to large declines in %MS/BS ($p < 0.0001$, effect size = 0.770), while MAR was not different between CON and SCI ($p = 0.251$). Endocortical BFR/BS at the midshaft tibia was lower, but not statistically different between SCI and CON ($p = 0.09$; Fig. 4B) with no statistical differences in MS/BS ($p = 0.112$) and MAR ($p = 0.057$).

3.6. Osteocyte density was not different between SCI and CON

Osteocyte density per tissue area (mm^2) in the distal femur was lower in SCI vs. CON (CON average = 602 ± 148, SCI average = 305 ± 100; $p = 0.002$, effect size = 0.622) while osteocyte density normalized to the bone area not different in SCI vs. CON (CON average = 39 ± 3, SCI average = 32 ± 10; $p = 0.195$). At the midshaft femur, osteocyte density was also not statistically different between CON and SCI (CON average = 355 ± 28, SCI average = 325 ± 19; $p = 0.100$).

3.7. SCI resulted in increased prevalence of pro-inflammatory osteocyte proteins, osteoclastogenesis regulator proteins, and sclerostin

In the cancellous bone, %TNF+ osteocytes in SCI animals were statistically higher than in CON ($p = 0.008$, effect size = 0.525; Fig. 5A), as were %IL-6+ osteocytes ($p < 0.0001$, effect size = 0.725; Fig. 5B). The SCI group had a higher percentage of osteocytes positive for both IL-10 ($p = 0.011$, effect size = 0.494; Fig. 5C) and IL-17

Table 2
pQCT measures of the midshaft tibia and midshaft femur assessed 32 days after moderate contusion injury at T12.

	Midshaft tibia		Midshaft femur	
	CON	SCI	CON	SCI
Cortical BMC (g)	6.72 ± 0.4	6.21 ± 0.4#	10.42 ± 0.7	9.4 ± 0.9#
Cortical vBMD (mg/cm^3)	1362.96 ± 46.8	1340 ± 17.2	1417.94 ± 15.2	1430.98 ± 10.8
Total area (mm^2)	7.4 ± 1.3	7.53 ± 1.2	10.93 ± 0.4	9.73 ± 0.5*
Cortical thickness (mm)	0.66 ± 0.06	0.59 ± 0.04#	0.79 ± 0.06	0.76 ± 0.08

Data are represented as mean ± standard deviation.
* Difference from CON, $p < 0.05$.
# Trending difference from CON, $p = 0.09$–0.05.

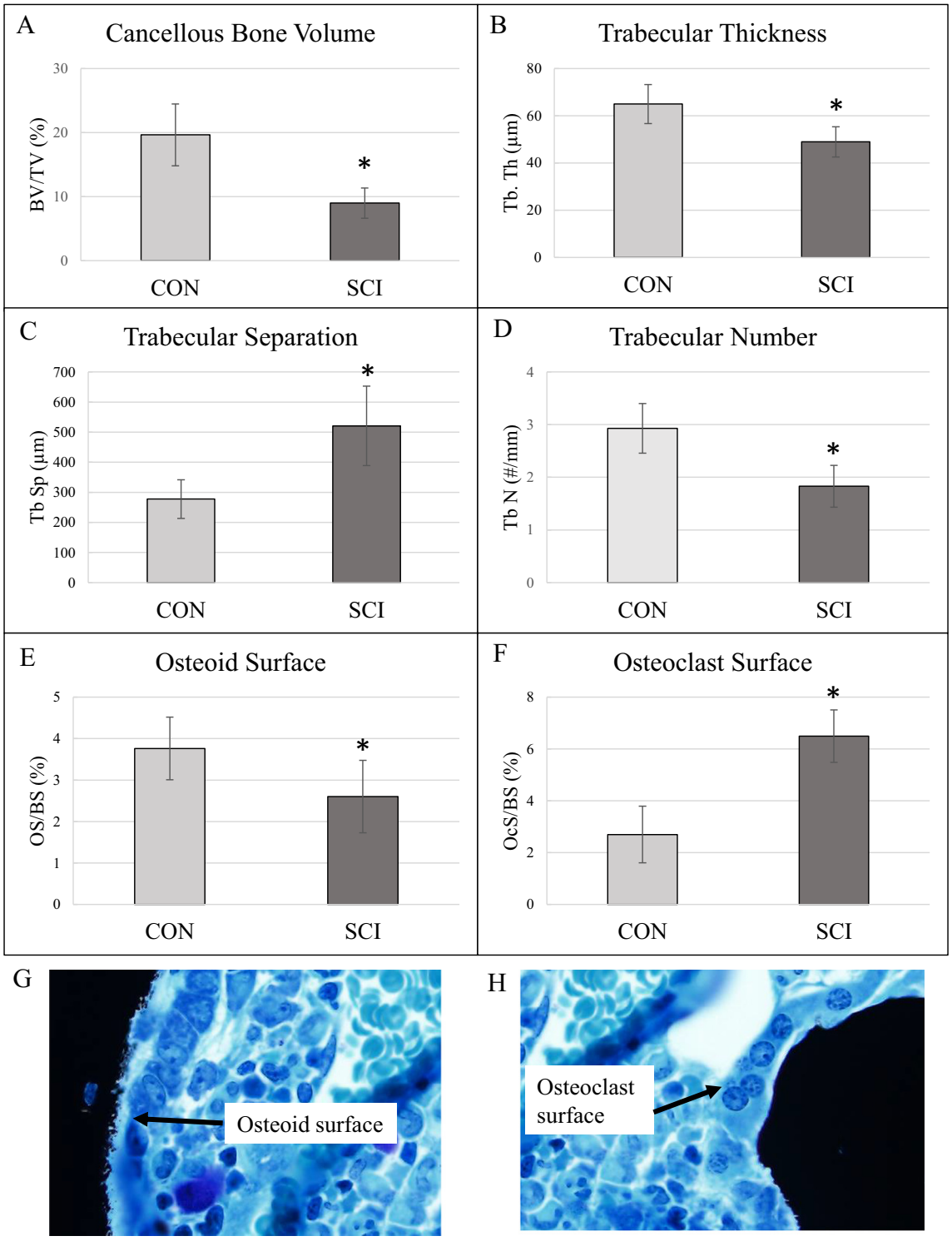

Fig. 2. Static histomorphometry at the proximal tibia metaphysis revealed lower cancellous bone volume, altered microarchitecture, high osteoclast surface, and low osteoid surface in SCI animals. A) Cancellous bone volume was lower in SCI vs. CON ($p = 0.001$). B) Trabecular thickness was lower in SCI vs. CON ($p = 0.004$). C) Trabecular separation was higher in SCI ($p = 0.002$). D) Trabecular number was lower in SCI vs. CON ($p = 0.001$). E) Cancellous osteoid surface (OS/BS) was lower in SCI ($p = 0.034$). F) Cancellous osteoclast surface (Oc.S/BS) was higher in SCI vs. CON ($p < 0.0001$). G) Representative image of osteoid surface at 40× magnification. H) Representative image of osteoclast surface at 40× magnification. *Statistically different from CON.

($p = 0.002$, effect size = 0.647; Fig. 5D). %RANKL- and %OPG-positive osteocytes were also higher in SCI vs. CON ($p = 0.003$, effect size = 0.603; $p = 0.001$, effect size = 0.790, respectively; Fig. 5E, F), as were %sclerostin+ osteocytes ($p = 0.007$, effect size = 0.533; Fig. 5G). In the cortical bone of the midshaft, %TNF-α+ osteocytes were higher in SCI vs. CON ($p = 0.016$, effect size = 0.491) as were % IL-6+ osteocytes ($p = 0.009$, effect size = 0.513) and %sclerostin+ osteocytes ($p = 0.002$, effect size = 0.725; Table 3). RANKL and OPG were undetectable in CON cortical midshaft sections, but were present in half of SCI samples (Table 3). IL-10 and IL-17 were not detectable in any midshaft section (Table 3).

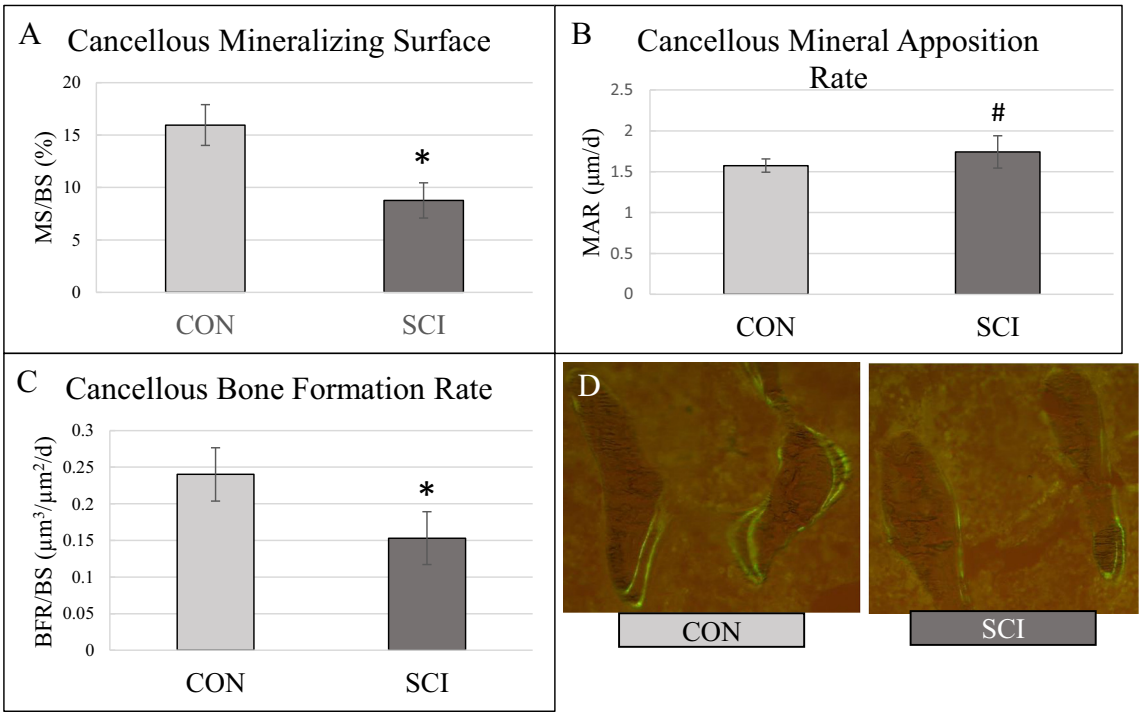

Fig. 3. Bone formation rate at the proximal tibia metaphysis is lower in SCI due to declines in mineralizing surfaces. A) Mineralized surface was lower in the cancellous bone of SCI rats compared to CON ($p < 0.0001$). B) Mineral apposition rate at the proximal tibia metaphysis did not reach statistical significance at $p < 0.05$, but SCI was trending higher ($p = 0.084$). C) Cancellous bone formation rate was lower in SCI vs. CON ($p = 0.002$). D) Representative image of cancellous fluorochrome labels (image at 20×). *Statistically different from CON. #$p = 0.084$.

3.8. Linear regression models demonstrate that inflammatory status is associated with bone outcomes

Sclerostin+ osteocytes are associated with TNF-α+ osteocytes ($R^2 = 0.770$, $p < 0.0001$; Fig. 6). Additionally, statistically significant regressions were found for osteoclast surface predicted by TNF-α+ osteocytes ($R^2 = 0.633$, $p = 0.002$), IL-6+ osteocytes ($R^2 = 0.674$, $p = 0.001$), IL-17+ osteocytes ($R^2 = 0.540$, $p = 0.006$), RANKL+ osteocytes ($R^2 = 0.346$, $p = 0.044$), and OPG+ osteocytes ($R^2 = 0.598$, $p = 0.003$; Fig. 6). No multiple linear regression models met our criteria for acceptance.

4. Discussion

The primary finding of this study is that pro-inflammatory markers are elevated in osteocytes concurrent with alterations in regulators of bone turnover. To the authors' knowledge, this study is the first to examine the impact of the protracted inflammatory status of SCI on bone outcomes. Our data indicates that inflammation could be a contributor to the significant and prolonged bone loss that occurs in SCI patients.

Bone loss caused by SCI is complex, since these injuries entail many neurological and physiological changes that evolve post-injury, as well as loss of mechanical loading. Adding to the complexity of studying SCI-induced bone loss in humans are differences in the level of injury and even the motor and sensory impairments at the same level of injury across individual patients. Animal models can help elucidate some of the factors associated with SCI by allowing for control over the spinal level and type of injury. The animals in our study had a moderate contusion injury resulting in approximately 55% lower cancellous bone volume with 25% lower trabecular thickness, nearly 90% greater trabecular separation, and 38% lower trabecular number 32 days following injury. Our histomorphometric data indicate that a large increase in osteoclasts and a modest reduction in bone formation rate drove this bone loss; there was a 37% decrease in cancellous bone formation rate and a 140% increase in osteoclast surface in SCI rats versus intact control rats. The directionality of these changes are similar to other rodent models of SCI [12,14], but the magnitude of change in our rats was less than that reported in more severe injury models. Similar analyses of iliac crest bone biopsies from immobilized human patients, the majority of whom had SCI, reveal large reductions in cancellous osteoid surface and higher osteoclast surfaces, particularly in the acute phase following the injury [39]. Tetracycline labeling in this same cohort of patients demonstrated extremely low mineral apposition rates [39].

Another rodent study utilizing a more severe contusion injury demonstrated > 70% reductions in cancellous bone volume with concurrent significant deteriorations in cancellous microarchitecture 21 days after injury [14]. Complete transection of the spinal cord in rats, which produces a motor-complete injury, results in approximately 67% lower cancellous bone volume 56 days following SCI [12]. These data in combination with those in the present study indicate that the severity and completeness of the injury determine the magnitude of deficits in bone parameters. It should be noted that the majority of our study's animals with a moderate contusion injury regained weight-bearing capacity by day 9 following injury, while animals with more severe contusion injuries do not regain weight-bearing by day 21 [14]. Nonetheless, the cancellous bone loss in our moderate SCI model was two-fold higher than the ~25% lower cancellous bone volume seen in skeletally mature rats after 28 days of hindlimb unloading versus weight-bearing controls [36]. This study's results are consistent with those of other animal studies indicating that the rapid and severe bone loss that occurs after SCI is greater than that seen with unloading/immobilization or loss of neural signaling (via neurectomy) alone [17,18].

Patients with SCI have long-term immune dysfunction and inflammation following injury [19]. Damage to sympathetic neurons innervating lymphoid organs and disruption of the hypothalamic-pituitary-adrenal axis could both be contributors to the immune alterations following SCI [19]. C-reactive protein (CRP) is higher in SCI patients

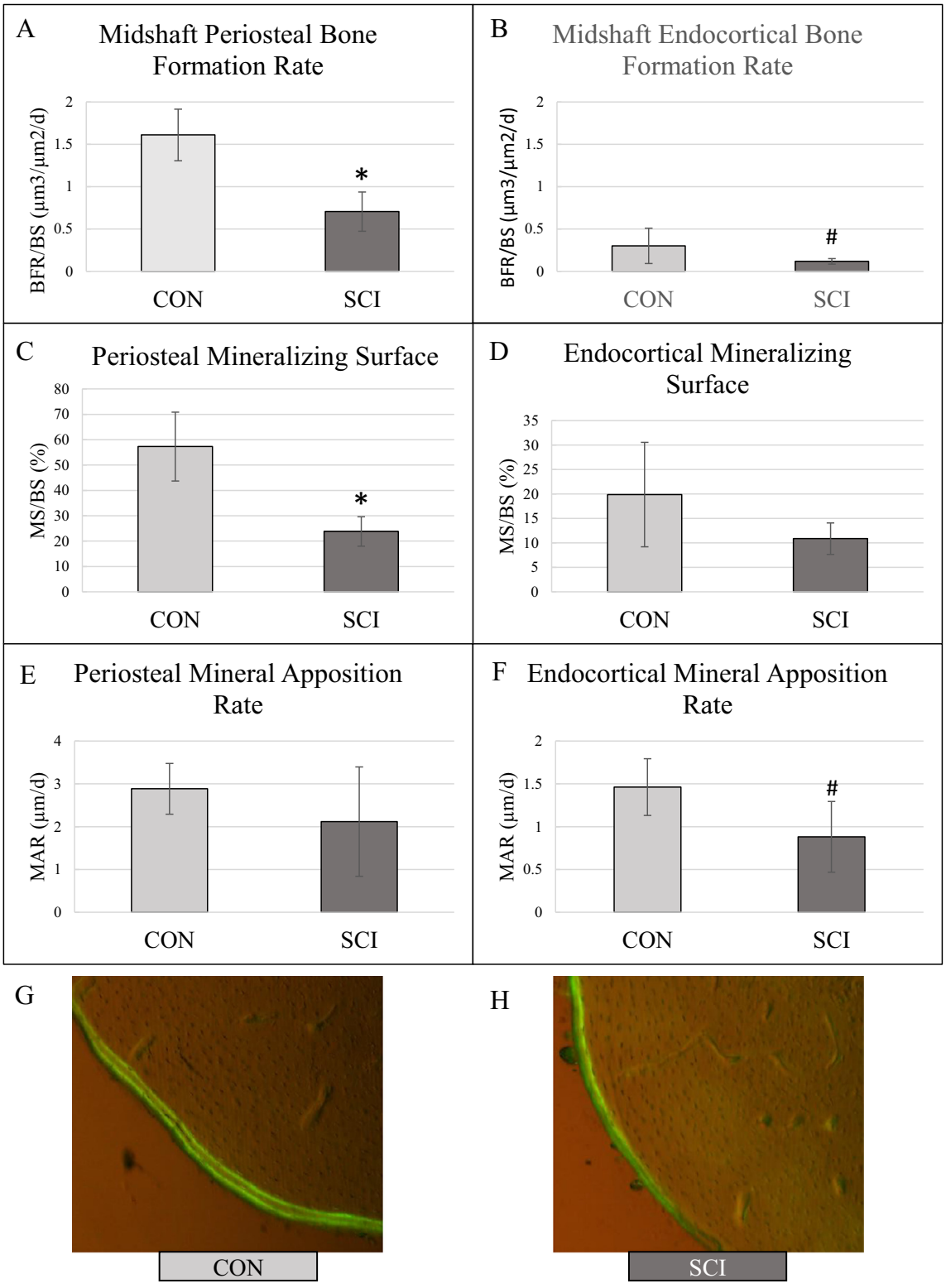

Fig. 4. Midshaft tibia periosteal bone formation rate was lower in SCI vs. Con. A) Periosteal BFR was lower in SCI vs. CON ($p < 0.0001$). B) Endocortical bone formation rate was lower in SCI, but not statistically different ($p = 0.09$). C) Periosteal mineralizing surface was lower in SCI vs. CON ($p < 0.0001$). D) Endocortical mineralizing surface was not different between groups. E) Periosteal mineral apposition rate was not different between groups. F) Endocortical mineral apposition rate was lower in SCI, but not statistically different ($p = 0.057$) G) Representative image of periosteal fluorochrome labels in CON at the midshaft tibia (image at 10×). H) Representative image of periosteal fluorochrome labels in SCI at the midshaft tibia (image at 10×). *Statistically different from CON at $p < 0.05$. #$p = 0.09–0.057$.

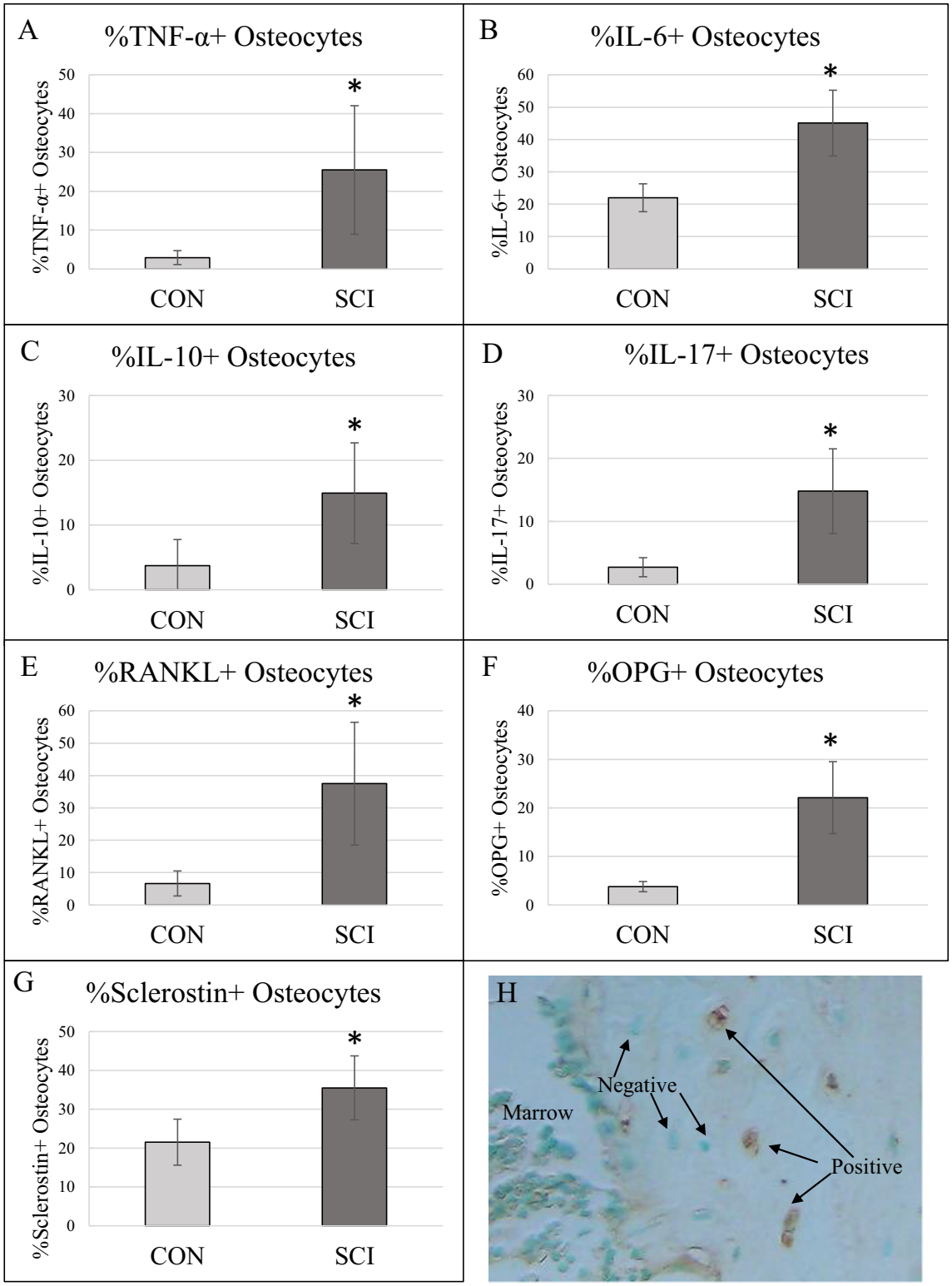

Fig. 5. Elevated pro-inflammatory factors and bone signaling proteins in the distal femur cancellous bone of SCI rats. A) %TNF-α+ osteocytes were higher in SCI vs. CON ($p = 0.008$). B) %IL-6+ osteocytes were higher in SCI ($p < 0.0001$). C) %IL-10+ osteocytes were higher in SCI than in CON ($p = 0.011$). D) %IL-17+ osteocytes were higher in SCI vs. CON ($p = 0.002$). E) SCI animals had higher %RANKL+ osteocytes than did CON ($p = 0.003$). F) SCI animals had higher %OPG+ osteocytes ($p = 0.001$). G) %sclerostin+ osteocytes were higher in SCI vs. CON ($p = 0.007$). H) Representative image of cancellous osteocytes with osteocytes stained positively (DAB; brown) for the protein of interest and negatively (methyl green; green). *Statistically different from CON. (For interpretation of the references to color in this figure legend, the reader is referred to the web version of this article.)

Table 3
Immunohistochemistry for osteocyte proteins in the midshaft femur.

Protein	CON	SCI
%TNF-α+	0.30 ± 0.2	5.24 ± 4.1*
%IL-6+	5.81 ± 1.7	12.13 ± 4.4*
%IL-10+	ND	ND
%IL-17+	ND	ND
%RANKL+	ND	6.62 ± 4.8
%OPG+	ND	3.69 ± 2.5
%Sclerostin+	28.86 ± 3.3	45.57 ± 7.4*

ND = not detectable in the region of interest. Statistics were not completed on variables with one group ND. Data are represented as mean ± standard deviation.

* Different from CON, $p < 0.05$.

compared to age-matched values even 10+ years following injury [26,28]. Additionally, circulating pro-inflammatory cytokines are higher in SCI patients in the chronic phase of SCI [29,30]. In a cohort of SCI patients (> 12 months following injury), 57% of the patients had high serum levels of pro-inflammatory cytokines or autoantibodies [30]. In another cohort of SCI patients on average 10 years following injury, elevated circulating levels of TNF-α and IL-6 were found even in patients asymptomatic for medical complications [29]. Given that chronic inflammatory conditions such as inflammatory bowel disease and psoriasis are associated with significant bone loss [20,21], it is reasonable to conjecture that the chronic pro-inflammatory state observed in individuals with SCI could account for the devastating rate of bone loss when compared to disuse alone (e.g., prolonged bedrest).

Previously, in an animal model of inflammatory bowel disease we found that osteocyte proteins reflected a pro-inflammatory state and these osteocyte proteins corresponded with changes in bone turnover [36]. In our SCI rats, we found nearly 12-fold higher TNF-α-positive osteocytes and 2-fold higher IL-6-positive osteocytes. TNF-α potently stimulates osteoclastogenesis [32,33,40,41] as well as inhibiting osteoblasts [32,42,43] and triggering osteoblast apoptosis [44]. IL-6 from osteocytes may signal to osteoblasts when acting alone [45] but, in the

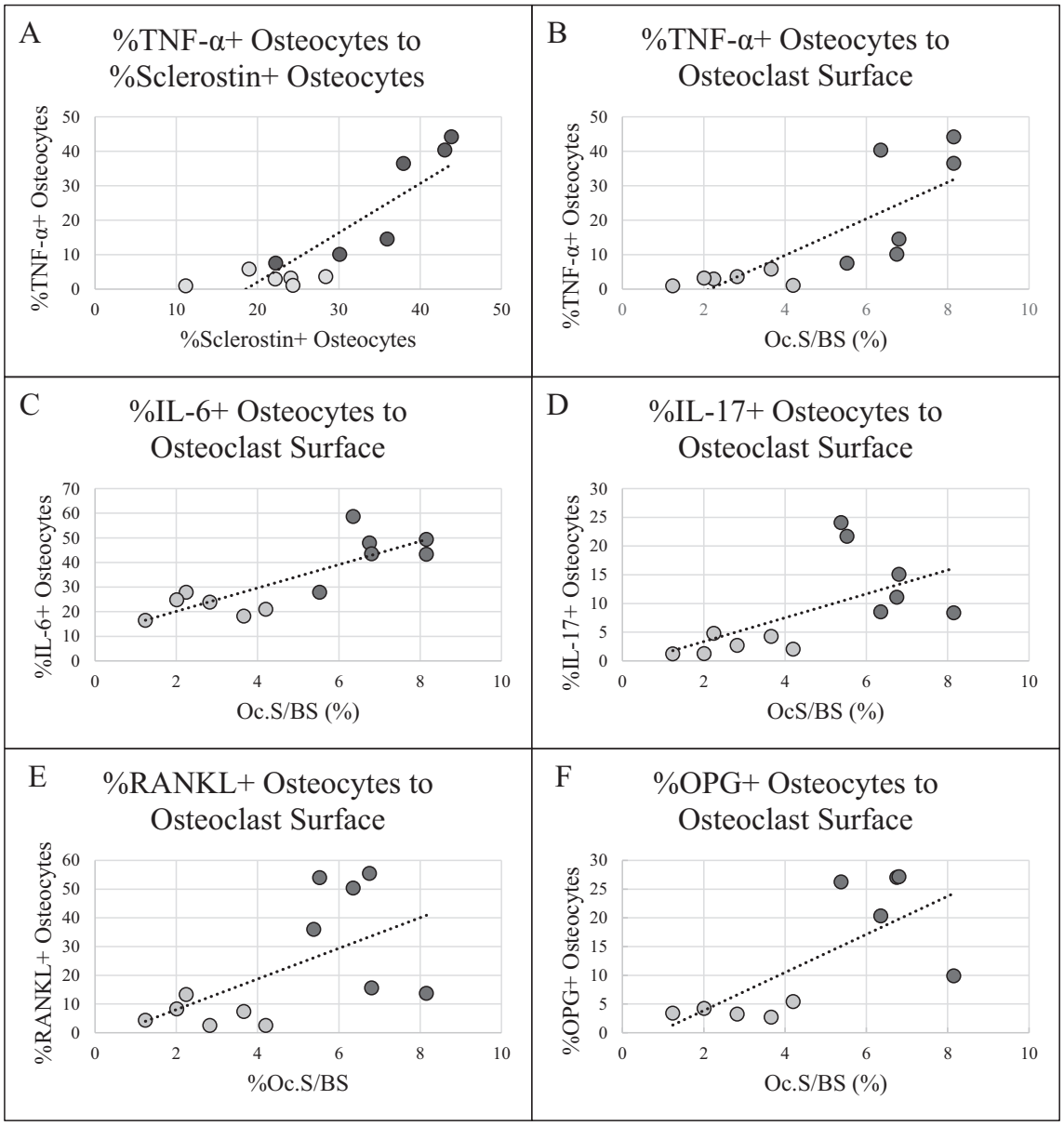

Fig. 6. Regression plots. A) %TNF-α+ osteocytes to %sclerostin+ osteocytes ($R^2 = 0.770$), B) %TNF-α+ osteocytes to osteoclast surface ($R^2 = 0.633$), C) %IL-6+ osteocytes to osteoclast surface ($R^2 = 0.674$), D) %IL-17+ osteocytes to osteoclast surface ($R^2 = 0.540$), E) %RANKL+ osteocytes to osteoclast surface ($R^2 = 0.346$), F) %OPG+ osteocytes to osteoclast surface ($R^2 = 0.598$). Dark markers = SCI, light markers = CON.

presence of TNF-α, IL-6 stimulates osteoclasts in a synergistic fashion [33]. These changes in osteocyte TNF-α and IL-6 in our rats are consistent with the high osteoclast surface and low osteoid surface and bone formation rate in the SCI animals. Previously, we demonstrated in skeletally mature hindlimb unloaded rats that osteocyte IL-6 is lower due to unloading and TNF-α remain unchanged [36]. Therefore, we hypothesize the changes we are seeing in SCI are due to both chronic systemic inflammation and lack of mechanical unloading, as the directionality of changes in TNF-α and IL-6 in our SCI animals is similar to what we have seen in our rats with inflammatory bowel disease [35]. Additionally, in our SCI rats, the number of osteocytes positive for interleukin-17 (IL-17) was 5-fold higher compared to intact control rats. IL-17, a Th17 cytokine, is known to be a potent stimulator of osteoclasts in conditions like rheumatoid arthritis [46]. Interestingly, interleukin-10, a Th2 cytokine that inhibits osteoclastogenesis in vitro [47,48], was also higher in SCI rats compared to controls. The role of IL-10 in bone physiology is still equivocal and the importance of osteocyte IL-10 is unknown. In our study, osteocytes positive for TNF-α, IL-6, and IL-17 were all associated with elevated osteoclast surface ($R^2 = 0.633$, $R^2 = 0.674$, $R^2 = 0.540$, respectively).

Osteocytes are now believed to have key regulatory roles in bone due to their ability to release signaling proteins and maintain a vast communication network through their dendritic processes with other osteocytes and other cells. Utilizing scanning electron microscopy, Qin et al determined that osteocytes following spinal cord transection had fewer dendritic processes and altered cell morphology compared to controls [12]. These same rats had no differences in osteocyte density per bone area than did control rats. We found similar changes in our SCI rats with no changes in osteocyte density normalized to bone volume in the cancellous bone and no differences in the cortical shaft. Interestingly, hindlimb unloading to induce disuse bone loss does result in lower cancellous osteocyte density in rats [36], alluding to potentially different mechanisms resulting in osteocyte apoptosis.

Osteocytes release proteins that signal to osteoblasts or osteoclasts to control bone turnover. Some of these proteins, such as RANKL, OPG, and sclerostin, are known to be mechanosensitive and respond to altered mechanical loading [36,49–51]. These signaling proteins are also influenced by inflammation. RANKL production is increased in the presence of TNF-α and IL-6 [33] and these factors synergistically work to increase osteoclastogenesis [32,33]. OPG, the decoy receptor for RANKL, is also upregulated by TNF-α [52]. In our rats, cancellous RANKL+ osteocytes were > 5-fold higher in SCI and OPG+ osteocytes were nearly 6-fold higher than in intact control rats. These changes corresponded with high cancellous osteoclast surface in SCI rats. Sclerostin, an inhibitor of bone formation, is transcriptionally activated by TNF-α [34] as well as upregulated by mechanical unloading [36]. In our SCI rats, cancellous sclerostin+ osteocytes were 66% higher compared to controls. TNF-α+ osteocytes were associated with higher osteocyte sclerostin ($R^2 = 0.716$, $R^2 = 0.770$, respectively). These changes in osteocyte RANKL, OPG, and sclerostin were similar to those seen in rats with chronic inflammatory bowel disease indicating the influence of inflammation in this model of SCI. These data indicate that both the inflammatory status of SCI and mechanical loading alterations influence osteocyte regulators of bone turnover.

Typically bone loss following SCI occurs rapidly in cancellous bone regions following the injury with slow, persistent bone loss in the cortical bone over time leading to increased fracture risk with time from injury [8]. In our rats, periosteal bone formation rate in SCI rats at the midshaft tibia was 56% with 10% lower cortical thickness compared to controls. We found elevations in TNF-α-, RANKL-, and sclerostin-positive osteocytes at the midshaft femur in SCI rats compared to control rats but, generally, we found more profound changes in osteocyte proteins at the cancellous bone. We hypothesize that our moderate SCI model, which resulted in moderate cancellous bone loss and some recovery of weight-bearing, produces less drastic cortical bone changes than would be seen in more severe injury models. Nonetheless, our data indicate that cortical bone was also affected by SCI, and may continue to develop, possibly due in part to inflammatory mechanisms. Further examination of bone loss in more chronic stages of injury is warranted.

Limitations of this study include comparison of SCI animals to intact controls without a sham surgery. Therefore, we cannot decipher what inflammatory changes are due to the surgery itself; however, the prolonged inflammatory changes seen 32 days after the spinal contusion we believe are indicative of the spinal cord injury, not the surgical procedure. When comparing to other models of SCI, it is also important to note that post-operative pain medications or NSAIDS were not given which may have influenced the inflammatory results in comparison to other studies. Another limitation is the inability to measure circulating serum cytokines in these animals due to the tissue-sharing nature of the protocol (serum samples were not available). However, we have previously demonstrated that age-matched rats with similar contusion injuries exhibited altered serum cytokine profiles compared to those of intact controls [31]. Future studies should address the time-course of development of inflammation in SCI and the response of osteocytes to this inflammation. Additionally, more mechanistic studies examining the interactions of cytokines, osteocytes, and other bone cells need to be addressed. It will be important to understand whether changes in osteocytes are mediating changes in other cells. Furthermore, the inflammatory impact on bone health may be of different magnitudes with different severities or spinal cord levels of injury. Nonetheless, our data support a potential role of inflammation contributing to bone loss during moderate SCI.

This study provides evidence for elevated pro-inflammatory cytokines in osteocytes one month following spinal cord injury and these changes are associated with alterations in bone turnover. Therefore, we conclude that likely both the lack of mechanical loading and protracted inflammation contribute to bone loss in SCI. Treatments to protect bone mass in SCI may need to address the chronic systemic inflammation that is prevalent in SCI to minimize loss of bone mass and better prevent fractures.

Acknowledgements

The animal work for this study was supported by Gilson-Longenbaugh Foundation and Mission Control (to MAH).

Authors' roles

CEM and MAH designed the hypotheses for this study and interpreted the data. CEM completed the analyses, ran statistical analyses, and wrote the manuscript. MAH designed and supervised the parent animal protocol and assisted in writing the manuscript. MA ran the animal protocol and edited the manuscript. SG assisted with running the animal protocol and completion pQCT and cortical BFR analyses and edited the manuscript. SAB edited the manuscript and assisted with interpretation of the data. All authors approved the final version.

References

[1] M.G. Lazo, P. Shirazi, M. Sam, A. Giobbie-Hurder, M.J. Blacconiere, M. Muppidi, Osteoporosis and risk of fracture in men with spinal cord injury, Spinal Cord 39 (2001) 208–214.
[2] F. Biering-Sørenson, H.H. Bohr, O.P. Schaadt, Longitudinal study of bone mineral content in the lumbar spine, the forearm and the lower extremities after spinal cord injury, Eur. J. Clin. Investig. 20 (1990) 330–335.
[3] P. Eser, A. Frotzler, Y. Zehnder, L. Wick, H. Knecht, J. Denoth, H. Schiessl, Relationship between the duration of paralysis and bone structure: a pQCT study of spinal cord injured individuals, Bone 34 (2004) 869–880.
[4] W. Qin, W.A. Bauman, C. Cardozo, Bone and muscle loss after spinal cord injury: organ interactions, Ann. N. Y. Acad. Sci. 1211 (2010) 66–84.
[5] W.A. Bauman, A.M. Spungen, J. Wang, R.N. Pierson, E. Schwartz, Continuous loss of bone during chronic immobilization: a monozygotic twin study, Osteoporos. Int. 10 (1995) 123–127.
[6] P. Vestergaard, K. Krogh, L. Rejnmark, L. Mosekilde, Fracture rates and risk factors for fractures in patients with spinal cord injury, Spinal Cord 36 (1998) 790–796.

[7] R.A. Battaglino, A.A. Lazzari, E. Garshick, L.R. Morse, Spinal cord injury-induced osteoporosis: pathogenesis and emerging therapies, Curr. Osteoporos. Rep. 10 (2012) 278–285.

[8] Y. Zehnder, M. Lüthi, M. Dieter, H. Knecht, R. Perrelet, I. Neto, M. Kraenzlin, G. Za, K. Lippuner, Long-term changes in bone metabolism, bone mineral density, quantitative ultrasound parameters, and fracture incidence after spinal cord injury: a cross-sectional observational study in 100 paraplegic men, Osteoporos. Int. 15 (2004) 180–198.

[9] L.A. Beggs, F. Ye, P. Ghosh, D.T. Beck, C.F. Conover, A. Balaez, J.R. Miller, E.G. Phillips, N. Zheng, A.A. Williams, I. Aguirre, T.J. Wronski, P.K. Bose, S.E. Borst, J.F. Yarrow, Sclerostin inhibition prevents spinal cord injury-induced cancellous bone loss, J. Bone Miner. Res. 30 (4) (2015) 681–689.

[10] L. Morse, Y.D. Teng, L. Pham, K. Newton, D. Yu, W.L. Liao, T. Kohler, R. Müller, D. Graves, P. Stashenko, R. Battaglino, Spinal cord injury causes rapid osteoclastic resorption and growth plate abnormalities in growing rats (SCI-induced bone loss in growing rats), Osteoporos. Int. 19 (2008) 645–652.

[11] S. Picard, N.P. Lapointe, J.P. Brown, P.A. Guertin, Histomorphometric and densitometric changes in the femora of spinal cord transected mice, Anat. Rec. 291 (2008) 303–307.

[12] W. Qin, X. Li, Y. Peng, L.M. Harlow, Y. Ren, Y. Wu, J. Li, Y. Qin, J. Sun, S. Zheng, T. Brown, J.Q. Feng, H.Z. Ke, W.A. Bauman, Sclerostin antibody preserves the morphology and structure of osteocytes and blocks the severe skeletal deterioration after motor-complete spinal cord injury in rats, J. Bone Miner. Res. 30 (11) (2015) 1994–2004.

[13] Pan J. Sun Li, Y. Peng, Y. Wu, J. Li, X. Liu, Y. Qin, W.A. Bauman, C. Cardozo, M. Zaidi, W. Qin, Anabolic steroids reduce spinal cord injury-related bone loss in rats associated with increased Wnt signaling, J. Spinal Cord Med. 36 (6) (2013) 616–622.

[14] J.F. Yarrow, C.F. Conover, L.A. Beggs, D.T. Beck, D.M. Otzel, A. Balaex, S.M. Combs, J.R. Miller, F. Ye, I. Aguirre, K.G. Neuville, A.A. Williams, B.P. Conrad, C.M. Gregory, T.J. Wronski, P.K. Bose, S.E. Borst, Testosterone dose dependently prevents bone and muscle loss in rodents after spinal cord injury, J. Neurotrauma 31 (2014) 834–845.

[15] S.D. Jiang, L.S. Jiang, L.Y. Dai, Changes in bone mass, bone structure, bone biomechanical properties, and bone metabolism after spinal cord injury: a 6-month longitudinal study in growing rats, Calcif. Tissue Int. 80 (2007) 167–175.

[16] L.F. Bonewald, The amazing osteocyte, J. Bone Miner. Res. 26 (2) (2011) 229–238.

[17] S.D. Jiang, L.S. Jiang, L.Y. Dai, Spinal cord injury causes more damage to bone mass, bone structure, biomechanical properties and bone metabolism than sciatic neurectomy in young rats, Osteoporos. Int. 17 (2006) 1552–1561.

[18] D. Liu, C.Q. Zhao, H. Li, S.D. Jiang, L.S. Jiang, L.Y. Dai, Effects of spinal cord injury and hindlimb immobilization on sublesional and supralesional bones in young growing rats, Bone 43 (2008) 119–125.

[19] D.J. Allison, D.S. Ditor, Immune dysfunction and chronic inflammation following spinal cord injury, Spinal Cord 53 (2015) 14–18.

[20] M. Agrawal, S. Arora, J. Li, R. Rahmani, L. Sun, A.F. Steinlauf, J.I. Mechanick, M. Zaidi, Bone, inflammation, and inflammatory bowel disease, Curr. Osteoporos. Rep. (2011) 251–257.

[21] E.A.S. Attia, A. Khafagy, S. Abdel-Raheem, S. Fathi, A.A. Saad, Assessment of osteoporosis in psoriasis with and without arthritis: correlation with disease severity, Int. J. Dermatol. 50 (2011) 30–35.

[22] G. Haugeberg, T. Uhlig, J.A. Falch, J.I. Halse, T.K. Kvien, Bone mineral density and frequency of osteoporosis in female patients with rheumatoid arthritis, Arthritis Rheum. 43 (3) (2000) 522–530.

[23] I.E.M. Bultink, Osteoporosis and fractures in systemic lupus erthyematosus, Arthritis Care Res. 64 (1) (2012) 2–8.

[24] A.K. Kesani, J.C. Urquhart, N. Bedard, P. Leelapattana, F. Siddiqi, K.R. Gurr, C.S. Bailey, Systemic inflammatory response syndrome in patients with spinal cord injury: does its presence at admission affect patient outcomes? Clinical article, J. Neurosurg. Spine 21 (2) (2014) 296–302.

[25] J.C. Fleming, C.S. Bailey, H. Hundt, K.R. Gurr, S.I. Bailey, G. Cepinskas, A.R. Lawendy, A. Badhwar, Remote inflammatory response in liver is dependent on the segmental level of spinal cord injury, J. Trauma Acute Care Surg. 72 (5) (2012) 1194–1201.

[26] H. Liang, M.C. Mojtahedi, D. Chen, C.L. Braunschweigh, Elevated C-reactive protein associated with decreased high-density lipoprotein cholesterol in men with spinal cord injury, Arch. Phys. Med. Rehabil. 89 (2008) 36–41.

[27] T.D. Wang, Y.H. Wang, T.S. Huang, T.C. Su, S.L. Pan, S.Y. Chen, Circulating levels of markers of inflammation and endothelial activation are increased in men with chronic spinal cord injury, J. Formos. Med. Assoc. 106 (11) (2007) 919–928.

[28] A.E. Gibson, A.C. Buchholz, K.A. Martin Ginis, SHAPE-SCI Research Group, C-reactive protein in adults with chronic spinal cord injury: increased chronic inflammation in tetraplegia vs paraplegia, Spinal Cord 46 (2008) 616–621.

[29] A.L. Davies, K.C. Hayes, G.A. Dekaban, Clinical correlates of elevated serum concentrations of cytokines and autoantibodies in patients with spinal cord injury, Arch. Phys. Med. Rehabil. 88 (2007) 1384–1393.

[30] K.C. Hayes, T.C.L. Hull, G.A. Delaney, P.J. Potter, K.A.J. Sequeira, K. Campbell, P.G. Popovich, Elevated serum titers of proinflammatory cytokines and CNS autoantibodies in patients with chronic spinal cord injury, J. Neurotrauma 19 (6) (2002) 753–761.

[31] S. Maldonado-Bouchard, K. Peters, S.A. Woller, B. Madahian, U. Faghihi, S. Patel, S. Bake, M.A. Hook, Inflammation is increased with anxiety- and depression-like signs in a rat model of spinal cord injury, Brain Behav. Immun. 51 (2016) 176–195.

[32] M.S. Nanes, Tumor necrosis factor-α: molecular and cellular mechanisms in skeletal pathology, Gene 321 (2003) 1–15.

[33] K.T. Steeve, P. Marc, T. Sandrine, H. Dominique, F. Yannick, IL-6, RANKL, TNF-alpha/IL-1: interrelations in bone resorption pathology, Cytokine Growth Factor Rev. 15 (2004) 49–60.

[34] K. Baek, H.R. Hwang, H.J. Park, A. Kwon, A.S. Qadir, S.H. Ko, K.M. Woo, H.M. Ryoo, G.S. Kim, J.H. Baek, TNF-α upregulates sclerostin expression in obese mice fed a high-fat diet, Cell. Physiol. 229 (2014) 640–650.

[35] C.E. Metzger, A. Narayanan, D.C. Zawieja, S.A. Bloomfield, Inflammatory bowel disease in a rodent model alters osteocyte protein levels controlling bone turnover, J. Bone Miner. Res. 32 (4) (2017) 802–813.

[36] C.E. Metzger, J.E. Brezicha, J.P. Elizondo, S.A. Narayanan, H.A. Hogan, S.A. Bloomfield, Differential responses of mechanosensitive osteocyte proteins in fore- and hindlimbs of hindlimb-unloaded rats, Bone 105 (2017) 26–34.

[37] D.M. Basso, M.S. Beattie, J.C. Bresnahan, A sensitive and reliable locomotor rating scale for open field testing in rats, J. Neurotrauma 12 (1995) 1–21.

[38] D.W. Dempster, J.E. Compston, M.K. Drezner, F.H. Glorieux, J.A. Kanis, H. Malluche, P.J. Meunier, S.M. Ott, R.R. Recker, A.M. Parfitt, Standard nomenclature, symbols, and units for bone histomorphometry: a 2012 update of the report of the ASMBR histomorphometry nomenclature committee, J. Bone Miner. Res. 28 (1) (2013) 1–16.

[39] P. Minaire, P. Meunier, C. Edouard, J. Bernard, P. Courpron, J. Bourret, Quantitative histological data on disuse osteoporosis, Calcif. Tissue Res. 17 (1974) 57–73.

[40] K. Kobayashi, N. Takahashi, E. Jimi, N. Udagawa, M. Takami, S. Kotake, N. Nakagawa, M. Kinosaki, K. Yamaguchi, N. Shima, H. Yasuda, T. Morinaga, K. Higashio, T.J. Martin, T. Suda, Tumor necrosis factor-α stimulates osteoclast differentiation by a mechanism independent of the ODF/RANKL–RANK interaction, J. Exp. Med. 191 (2) (2000) 275–285.

[41] J. Lam, S. Takeshita, J.E. Barker, O. Kanagawa, F.P. Ross, S.L. Teitelbaum, TNF-α induces osteoclastogenesis by direct stimulation of macrophages exposed to permissive levels of RANK ligand, J. Clin. Invest. 106 (2000) 1481–1488.

[42] S. Abbas, Y.H. Zhang, J.C. Clohisy, Y. Abu-Amer, Tumor necrosis factor-α inhibits pre-osteoblast differentiation through its type-1 receptor, Cytokine 22 (2003) 33–41.

[43] H. Kaneki, R. Guo, D. Chen, Z. Yao, E.M. Schwarz, Y.E. Zhang, B.F. Boyce, L. Xing, Tumor necrosis factor promotes Runx2 degradation through up-regulation of Smurf1 and Smurf2 in osteoblasts, J. Biol. Chem. 281 (7) (2006) 4326–4333.

[44] F.M. Pavalko, R.L. Gerard, S.M. Ponik, P.J. Gallagher, Y. Jin, S.M. Norvell, Fluid shear stress inhibits TNF-a-induced apoptosis in osteoblasts: a role for fluid shear stress-induced activation of PI3-kinase and inhibition of caspase-3, J. Cell. Physiol. 194 (2002) 194–205.

[45] A.D. Bakker, R.N. Kulkarni, J. Klein-Nulend, W.F. Lems, IL-6 alters osteocyte signaling toward osteoblasts but not osteoclasts, J. Dent. Res. 93 (4) (2014) 394–399.

[46] S. Kotake, N. Udagawa, N. Takahashi, K. Matsuzaki, K. Itoh, S. Ishiyama, S. Saito, K. Inoue, N. Kamatani, M.T. Gillespie, T.J. Martin, T. Suda, IL-17 in synovial fluids from patients with rheumatoid arthritis is a potent stimulator of osteoclastogenesis, J. Clin. Invest. 103 (1999) 1345–1352.

[47] K.E. Evans, S.W. Fox, Interleukin-10 inhibits osteoclastogenesis by reducting NFATc1 expression and preventing its translocation to the nucleus, BMC Cell Biol. 8 (4) (2007).

[48] L.X. Xu, T. Kukita, A. Kukita, T. Otsuka, Y. Niho, T. Iijima, Interleukin-10 selectively inhibits osteoclastogenesis by inhibiting differentiation of osteoclast progenitors into preosteoclast-like cells in rat bone marrow culture system, Cell. Physiol. 165 (1995) 624–629.

[49] A.G. Robling, P.J. Niziolek, L.A. Baldridge, K.W. Condon, M.R. Allen, I. Alam, S.M. Mantila, J. Gluhak-Heinrich, T.M. Bellido, S.E. Harris, C.H. Turner, Mechanical stimulation of bone *in vivo* reduces osteocyte expression of Sost/sclerostin, J. Biol. Chem. 283 (9) (2008) 5866–5875.

[50] J. Xiong, M. Onal, R.L. Jilka, R.S. Weinstein, S.C. Manolagas, C.A. O'Brien, Matrix-embedded cells control osteoclast formation, Nat. Med. 17 (10) (2011) 1235–1241.

[51] L. You, S. Temiyasathit, P. Lee, C.H. Kim, P. Tummala, W. Yao, W. Kingery, A.M. Malone, R.Y. Kwon, C.R. Jacobs, Osteocytes as mechanosensors in the inhibition of bone resorption due to mechanical loading, Bone 42 (2008) 172–179.

[52] L.C. Hofbauer, C.R. Dunstan, T.C. Spelsberg, B.L. Riggs, S. Khosla, Osteoprotegerin production by human osteoblast lineage cells is stimulated by vitamin D, bone morphogenetic protein-2, and cytokines, Biochem. Biophys. Res. Commun. 250 (1998) 776–781.